Abstract

The flow over an isolated two-dimensional mountain is investigated using a vertical slice version of the Met Office Unified model. The upstream flow is of constant wind speed U and constant Brunt-Väisälä frequency N. The dimensionless parameters for this problem are the Froude number $Fr = U/NH$, Rossby number $Ro = U/fL$ and the ratio f/N, where L is the half-width of the mountain, f is the Coriolis parameter and H is the maximum height of the mountain. The solution is approximately determined by Ro and Fr if H/L is fixed. It is found that the limit $f \to 0$ is singular (i.e. the flow solution does

Contents

List of Symbols

D $P K \rho \rho$ $\rho P P j k \rho$ $k K \rho$ **Π Γ S**

List of Figures

List of Tables

Chapter 1

Introduction

The problem of stratified flow over mountains has been studied for several decades. A "classical" problem in this field of study is that of steady, Boussinesq, hydrostatic, non-rotating flow, unbounded above (Smith 1989).

There are a wide range of scales that must be considered, for example, the nature of a disturbance caused by a narrow hill is quite different to that of a broad plateau, even if the height of the terrain and other factors are the same. For small-scale mountains or hills which are $100m$ to $50km$ wide, the flow can be considered without including the Coriolis force. For mesoscale and synoptic-scale mountains (wider than $50km$) the rotation of the Earth cannot be neglected. Examples of such mountains include the Scandinavian mountain range (width $\sim 300km$), the Alps (width $\sim 250km$), and the Canadian Rockies (width $\sim 400km$) (Smith 1979b).

There are many features of airflow over mountains, both upstream and downstream of the mountain. A few examples include upstream blocking, barrier jets, gravity waves, trapped lee waves and föhn winds.

The blocking of low-level air is one of the most important ways in which mountains affect the air flow. The heavy surface air may have difficulty in running upslope and due to this, the surface level flow tends to slow as it approaches the mountain (Smith 1979a). In the nonrotating case this upstream layer of stagnant fluid will eventually be of infinite extent. However, in the rotating case the Coriolis force limits this extent to a maximum

Figure 1.1 indicates how the flow is influenced for different values of Ro and Fr.

Figure 1.1: *Influence of rotation and stratification on the flow as a function of Ro and Fr. (Adapted from Cushman-Roisin (1994))*

The problem considered in this project is that of a flow of constant speed with height (U) and constant stratification with height (N). This flow goes over an isolated, two-dimensional cosine mountain of half-width L and maximum height H (Fig. 1.2).

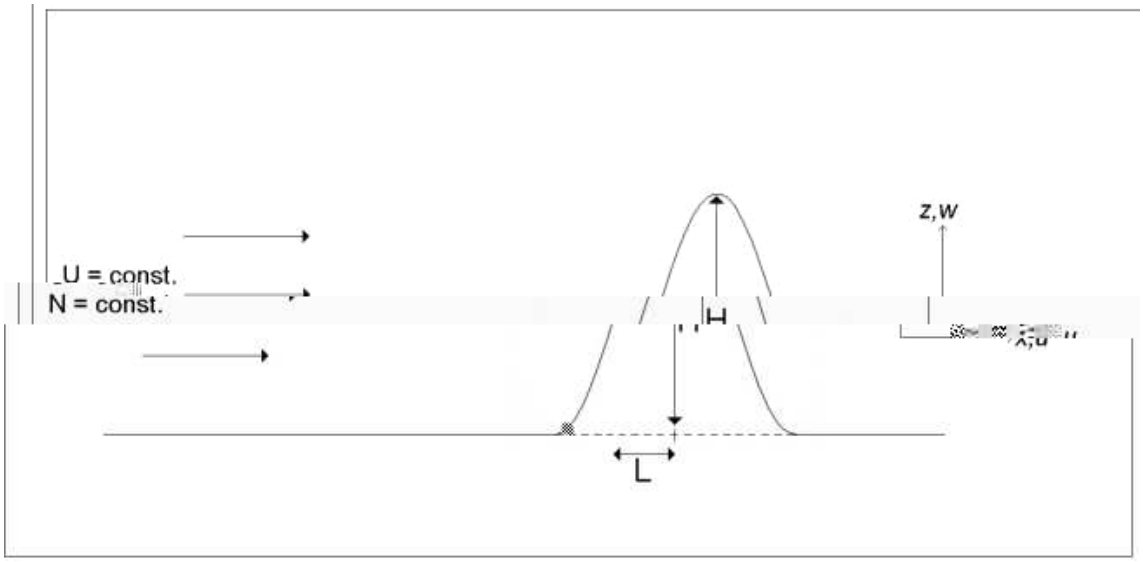

Figure 1.2: *Schematic of the flow problem considered in this project. The mountain is a cosine shape of half-width L and maximum height H. The upstream*

model is given by Cullen *et al.* (1997

Chapter 2

Linear Analysis of the Basic Equations

2.1

horizontal momentum equations, (2.3) is the vertical momentum equation, (2.4) is the thermodynamic equation and (2.5) is the mass conservation equation. These are the equations that are being solved by the model used in this project.

We now non-dimensionalise Eqs. (2.7) - (2.11) by using scalings of the form

$$u^* = Uu$$
$$v^* = Uv$$
$$w^* = Ww$$
$$t^* = Tt$$
$$x^* = Lx$$
$$y^* = Ly$$
$$z^* = Hz$$
$$\theta_1 = \theta_0\theta$$
$$p^* = Pp$$

and we choose $U = LT^{-1}$, $W = HT^{-1}$ and $P = L^2T^{-2}$.

By using the above scalings and multiplying through by T/U, the non-dimensional horizontal momentum equations become

$$\frac{u}{t} + u\frac{u}{x} + v\frac{u}{y} + w\frac{u}{z} + \frac{p}{x} - Ro^{-1}v = 0 \tag{2.12}$$

$$\frac{v}{t} + u\frac{v}{x} + v\frac{v}{y} + w\frac{v}{z} + \frac{p}{y} + Ro^{-1}u = 0 \tag{2.13}$$

and we see that the dimensionless Rossby number is now present as a control parameter. Doing the same as above but this time multiplying through by T/W, the non-dimensional vertical momentum equation becomes

$$\frac{w}{t} + u\frac{w}{x} + v\frac{w}{y} + w\frac{w}{z} + A^{-2}\frac{p}{z} - g\theta = 0 \tag{2.14}$$

where the aspect ratio g - g c C C C r c C

and

$$\frac{u}{x} + \frac{v}{y} + \frac{w}{z} = 0. \tag{2.16}$$

We now define the linearised, non-dimensional form of the Boussinesq hydrostatic balance approximation to be

$$A^{-2}\frac{\overline{p}}{z} = g\overline{\theta}. \tag{2.17}$$

We linearise about a state of rest ($p = \overline{p}(z)$, $\theta = \overline{\theta}(z)$) and divide the dependant variables into constant basic state portions (t v on r

and by using (2.17) we obtain the linearised vertical momentum equation

$$\frac{w'}{t} + A^{-2}\frac{p'}{z} - g\theta' = 0. \tag{2.20}$$

Finally, the linearised mass conservation and thermodynamic equations are

$$\frac{u'}{x} + \frac{v'}{y} + \frac{w'}{z} = 0 \tag{2.21}$$

$$\frac{\theta'}{t} + w'\frac{\overline{\theta}}{z} = 0 \tag{2.22}$$

respectively.

We see that the Froude number has not yet been introduced into the equations. To do this we take $\frac{\partial}{\partial t}$ of Eq. (2.20), giving

$$\frac{^2w'}{t^2} + A^{-2}\frac{^2p'}{z\ \ t} - g\frac{\theta'}{t} = 0.$$

Substituting in for $\frac{\partial\theta'}{\partial t}$ from Eq. (2.22) gives

$$\frac{^2w'}{t^2} + A^{-2}\frac{^2p'}{z\ \ t} + w'g\frac{\overline{\theta}}{z} = 0.$$

We now define

$$Fr^{-2} = g\frac{\overline{\theta}}{z}A^2$$

and note that

$$N^2 = g^*\frac{\overline{\theta}}{z^*} = T^{-2}Fr^{-2}A^{-2}$$

so

$$Fr^{-2} = N^2 T^2 A^2 = \frac{N^2 H^2}{U^2} \qquad \Rightarrow \qquad Fr = \frac{U}{NH}.$$

So Fr has been introduced into the equations after linearisation. Solutions of the nonlinear equations will thus depend only on Ro, A and g. If the linearisation is accurate, the solution will depend on Ro, A and Fr.

2.2 Solution of the linearised equations

We now assume solutions of the form

$$\begin{aligned} u &= \hat{u}\, e^{i(\omega t + kx + ly + mz)} \\ v &= \hat{v}\, e^{i(\omega t + kx + ly + mz)} \\ w &= \hat{w}\, e^{i(\omega t + kx + ly + mz)} \\ p &= \hat{p}\, e^{i(\omega t + kx + ly + mz)} \\ \theta &= \hat{\theta}\, e^{i(\omega t + kx + ly + mz)} \end{aligned}$$

and upon substitution these give

$$\begin{aligned} i\omega\hat{u} + ik\hat{p} - f\hat{v} &= 0 \\ i\omega\hat{v} + il\hat{p} + f\hat{u} &= 0 \\ i\omega\hat{w} + im\hat{p} - \frac{g\hat{\theta}}{\theta_0} &= 0 \\ ik\hat{u} + il\hat{v} + im\hat{w} &= 0 \\ i\omega\hat{\theta} + \frac{\overline{\theta}}{z}\hat{w} &= 0. \end{aligned}$$

Non-trivial solutions to this system of equations are given by

$$\det \begin{vmatrix} i\omega & -f & 0 & ik & 0 \\ f & i\omega & 0 & il & 0 \\ 0 & 0 & i\omega & im & -\frac{g}{\theta_0} \\ ik & il & im & 0 & 0 \\ 0 & 0 & \frac{\partial \overline{\theta}}{\partial z} & 0 & i\omega \end{vmatrix} = 0.$$

We assume that $N^2 \equiv \frac{g}{\theta_0}\frac{d\overline{\theta}}{dz}$ is independent of z and we obtain

$$-i\omega^3(k^2+l^2+m^2) + i\omega f^2 m^2 + i\omega(k^2+l^2)N^2 = 0$$

$$\Rightarrow \qquad \omega = 0 \qquad \text{or} \qquad \omega = \pm\sqrt{\frac{f^2m^2 + (k^2+l^2)N^2}{k^2+l^2+m^2}}. \tag{2.23}$$

We now define a characteristic time scale $T = \omega^{-1}$, horizontal length scale $L = (k^2+l^2)^{-\frac{1}{2}}$ and height scale $H = m^{-1}$. Three cases of (2.23) can be investigated as follows:

Case 1: $m^2 \gg k^2 + l^2$ *and* f ^{l}

Case 3: $m^2 \gg k^2 + l^2$ *but* $f^2 m^2 \ll (k^2 + l^2) N^2 \qquad (L/H \gg 1)$

In this case the solution reduces to

$$\omega = \pm \sqrt{\frac{(k^2 + l^2) N^2}{m^2}} \quad \Rightarrow \quad \frac{\omega}{\sqrt{k^2 + l^2}} = \frac{N}{m}$$

leading to internal gravity waves.

We expect these solutions to be typical of the wave solutions of the fully compressible equations.

2.3 Description of the semi-geostrophic solution

Shutts (

Chapter 3

Steady State Experiments

3.1 Overview of the model

The experiments in this project are conducted using a vertical slice version of the Met Office Unified model. The model makes use of a semi-implicit integration scheme and semi-Lagrangian advection (Cullen *et al.* 1997). There is no CFL criterion and so in the scheme u_j does not depend upon its immediate neighbours and thus there is no restriction on Δt. The idea of semi-Lagrangian schemes is to achieve stability even for large Δt by choosing the most appropriate interval for interpolation, so satisfying the CFL criterion. However, stability is still limited by a trajectory crossing condition. Some disadvantages of semi-Lagrangian schemes are that more computer time is required per time step, they are not particularly accurate with fast forcing such as semi-implicit gravity waves and they are overly diffusive on coarse grids.

Other features of the model are the inclusion of non-hydrostatic effects and the use of a semi-implicit algorithm for solving the fully compressible equations. Finite differences are used and the 'Charney-Phillips' vertical arrangement of variables (Fig. 3.1) is used to improve the geostrophic adjustment properties (Cullen *et al.* 1997).

The time integration scheme used in the model is based on the second order implicit Trapezoidal scheme

$$u^{n+1} = u^n + \frac{\Delta t}{2}[F(u^{n+1}) + F(u^n)]$$

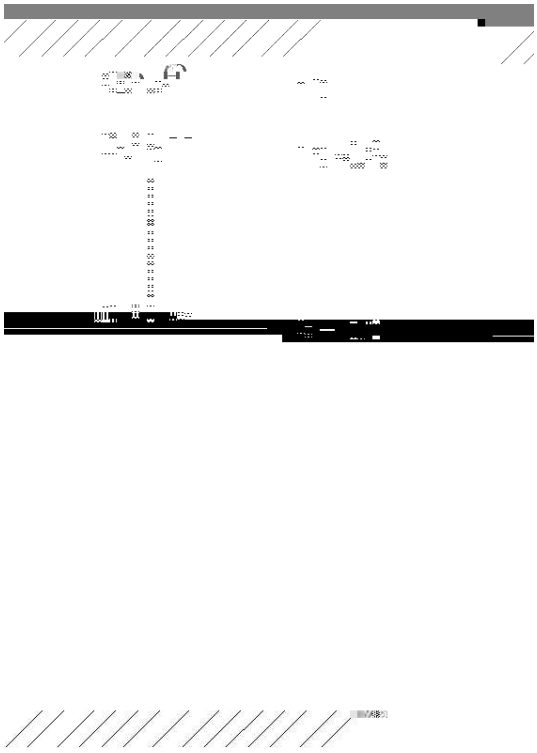

Figure 3.1: *Position of the variables of the Charney-Phillips grid where π = Exner pressure (taken from Cullen et al. (1997)).*

which is then generalised by

$$u^{n+1} = u^n + \frac{\Delta t}{2}[\alpha F(u^{n+1}) + (1-\alpha)F(u^n)]$$

where α is a weighting parameter between 0 and 1. Three choices of α can occur as follows:

$\alpha < \frac{1}{2}$	unstable
$\alpha = \frac{1}{2}$	scheme 2^{nd} order accurate
$\alpha > \frac{1}{2}$	damping occurs.

In this model the orography is grown in the first part of the run to ensure a smooth start.

3.2 Choice of CFL and α

An important consideration in all numerical modelling is how computationally expensive the model is, i.e. how much computer time is needed to achieve the required result. In the model used here the value of the CFL number determines the timestep. A larger CFL number will give a larger timestep. We obviously want to use as little computer time as possible and so we want to find the least number of timesteps and the longest timestep necessary for steady state, i.e. the solution in which the fields no longer vary with time. We require this steady state in order to see the response to the presence of the ridge.

The value of the weighting parameter α will also affect how quickly the solution reaches steady state. As stated in the previous section damping of the solution occurs for $\alpha > \frac{1}{2}$. So in this section we set the Coriolis parameter f to zero and investigate different values of CFL and α to see which combination gives the fastest convergence to steady state.

Values of CFL investigated here are 0.2 and 0.4. Higher values were tried but these caused the model to fail in the region of strong downslope winds. Values of α investigated are 0.8 and 1.0. To keep each experiment consistent we keep the product of CFL and the number of timesteps for the orography to grow to its final height, equal to 20. Thus for CFL = 0.2 the orography takes 100 timesteps to grow, and for CFL = 0.4 it takes 50 timesteps to grow.

Figure 3.2 shows graphs of how the u and w fields for each combination of CFL and α tend to steady state. We can see that for CFL = 0.4 the differences in the fields between time steps are less than for CFL = 0.2 from 150 time steps and from here these differences remain small and reasonably constant. Thus the solution tends to steady state in a lesser number of timesteps than for CFL = 0.2. Also, for CFL = 0.4 and for $\alpha = 1.0$ steady state is reached at the same time as for $\alpha = 0.8$ but the difference in each field between timesteps is slightly less.

For subsequent experiments in this project we therefore choose standard values of CFL = 0.4 and $\alpha = 1.0$.

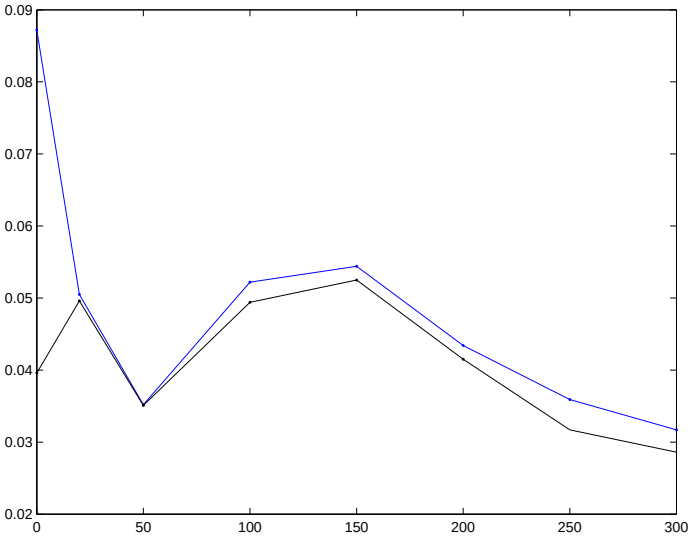
0.09
0.08
0.07
0.06
0.05
0.04
0.03
0.02
0
50
100
150
200
250
300

3.3 Steady state for $f \to 0$

In these experiments we now switch rotation on and attempt to find the steady state solution of flow over an isolated cosine hill of half-width $L = 300km$ and height $H = 2400m$. In the vertical the model has 20 levels with a grid length of $0.5km$. The horizontal grid length is $50km$.

For the steady state solution ($\frac{Dv}{Dt} = \frac{\partial v}{\partial t} + u\frac{\partial v}{\partial x} + w\frac{\partial v}{\partial z} = 0$) our y-component equation of motion (2.2) becomes

$$fU = -\frac{1}{\rho}\frac{p}{y} \tag{3.1}$$

where U is the wind speed in the x direction. As we keep U at a constant value of $10ms^{-1}$ and vary f we must also vary the right-hand side of (3.1) by the same factor so as to always keep the equation in balance. For example, if we halve the value of f we must also halve the value of the right-hand side.

From the linear analysis in Section 2.2 we can say that *Case 1* is applicable here because our mountain half-width $L = 300km$ and mountain height $H = 2400m$ ($L/H \gg 1$). This gave a characteristic timescale $T = f^{-1}$. The time to reach geostrophic balance will be of order this timescale and so the time for the solution to reach steady state should be a few times f^{-1}. This will increase with decreasing values of f and decrease with increasing values of f. However, the downstream flow is turbulent and so the solution will never reach steady state.

Table 3.1 gives the values of f used in this experiment. A value of $f = f_0/6$ was also tried but this solution did not converge to a steady state. Increasing the domain length further may have solved this problem but then the experiment would become too computationally expensive.

principle applies here as in the previous section in that if we halve the value of U we must also halve the value of the right-hand side.

Table 3.2: *Values of U used in experiment.*

U	Value
$2U_0$	$20ms^{-1}$
U_0	$10ms^{-1}$
$U_0/2$	$5ms^{-1}$
$U_0/4$	$2.5ms^{-1}$

Again, the time for the solution to reach steady state should be a few times f^{-1} and only the left half of the domain is considered when using (3.2).

Table 3.2 gives the values of U used in this experiment. The timestep is also determined by the value of U and so it is still necessary to do the steady state experiments even though f is being held constant. The model would not run for values of U smaller than $2.5ms^{-1}$ which may be due to the timestep becoming too large for the given Courant number. For $U = 2U_0, U_0, U_0/2, U_0/4$ the timesteps are $1012s$, $2025s$, $4050s$ and $8101s$ respectively. Therefore the times for the mountain to fully grow are $14.1hr$, $28.1hr$, $56.3hr$ and $112.0hr$ respectively.

Figure 3.4 shows graphs of how the u, v and w fields for each U tend to steady state. For $U = 2U_0, U_0, U_0/2, U_0/4$ the steady states are taken to be $112hr$ (400 timesteps), $112hr$ (200 timesteps), $112hr$ (100 timesteps) and $338hr$ (150 timesteps) respectively. Note that for the first three the time to reach steady state th Fssi sprin - e e seming g

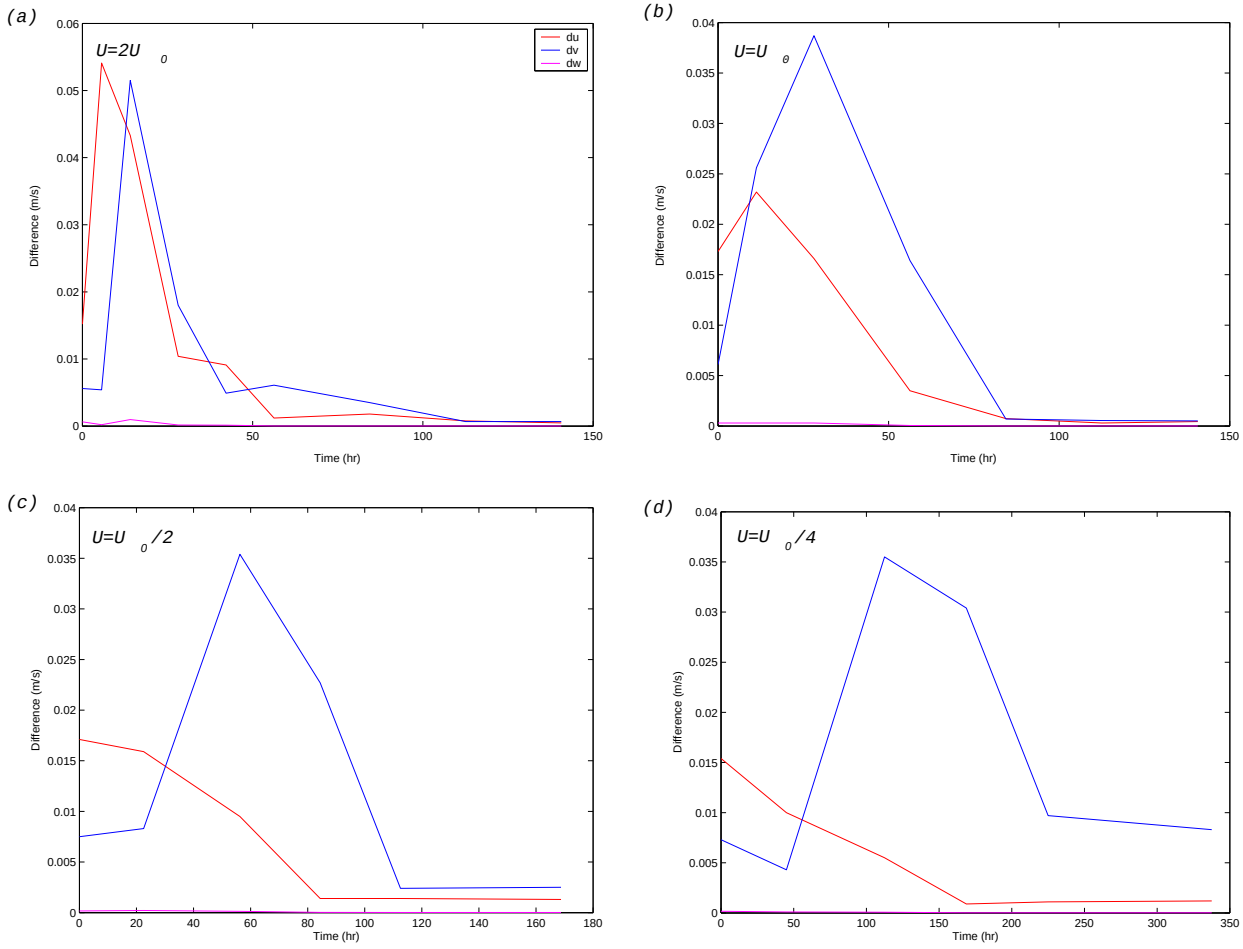

Figure 3.4: *Times for solution to reach steady state for (a) $2U_0$, (b) U_0, (c) $U_0/2$ and (d) $U_0/4$. The legend shown in (a) applies to all graphs.*

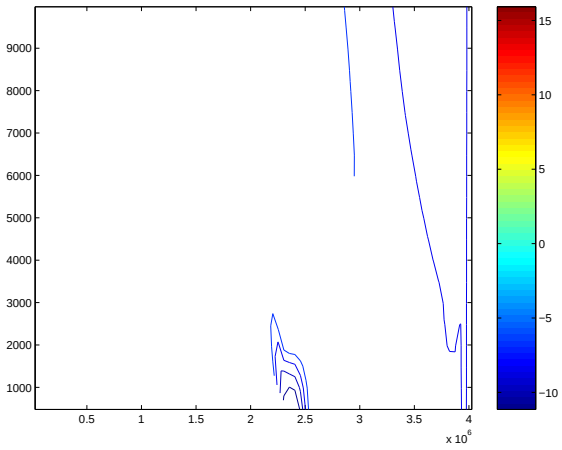
9000
8000
7000
6000
5000
4000
3000
2000
1000
0.5
1
1.5
2
2.5
3
3.5
4
x 10^6
15
10
5
0
−5
−10

1985). We can see from (4.1) that as f decreases L_R increases and so as $f \to 0$, $L_R \to \infty$. Similar results were found by Cullen *et al.* (1987). They conducted experiments with a stratified flow over a mountain barrier and in the absence of rotation they found no limit on the upstream influence as dense air was blocked by the mountain. With rotation present the upstream influence was restricted to a finite distance.

We can also measure the distance of upstream influence using

$$\delta x = \frac{v_{max}}{f} \tag{4.2}$$

where δx is the distance that an air parcel is 'pushed back from where it wants to be' by the orography, and v_{max} is the maximum wind speed in the barrier jet. We again see that as f decreases, this distance increases.

We now compare our results with the above theory. To begin with we can see a well defined barrier jet for each f value in Fig. 4.1 in the form of high v values on the upstream side of the mountain. This immediately agrees with the theory.

The distance of upstream influence for each f is found by calculating the horizontal upstream distance from the centre of the mountain that the value of v decreases to 10% of it's maximum value in the jet. We shall call this model-produced distance L_m.

The variation of L_m with f is shown in Fig. 4.3 along with the theoretical deformation radius L_R as given by (4.1). Also shown is the variation of δx as calculated using (4.2) with the model-produced values of v_{max}.

We can see that the distance δx is in close agreement with the theoretical L_R and that it decreases as f increases, as it should do. However, the distance L_m follows the same trend but has much larger values. The difference between L_m and L_R is of the order $1000km$.

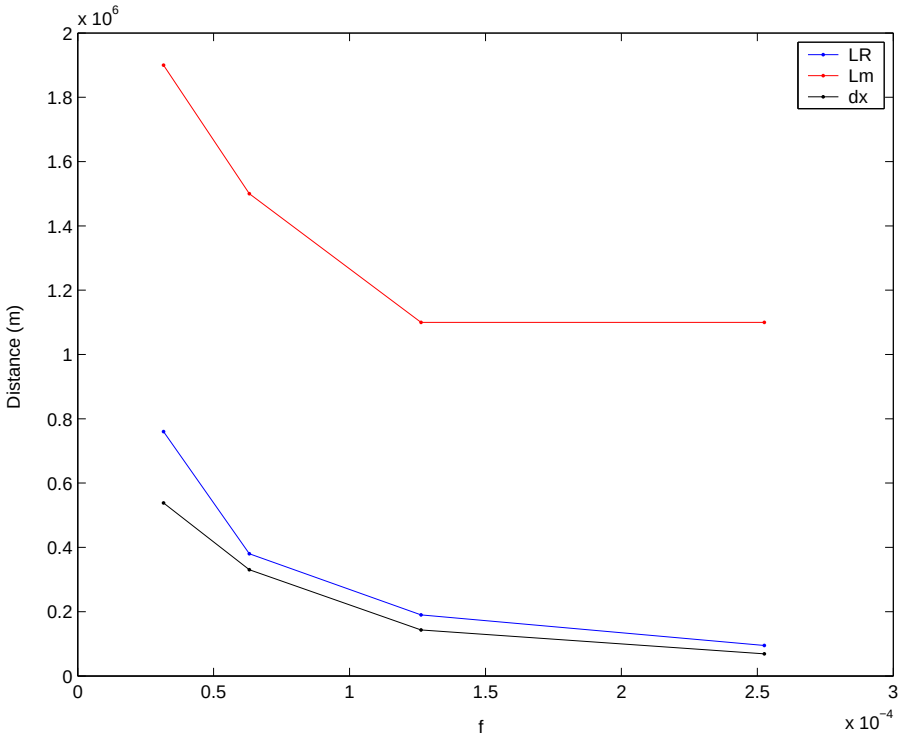
x 10^6
2
1.8
1.6
1.4
1.2
1
0.8
0.6
0.4
0.2
0
Distance (m)
0
0.5
1
1.5
2
2.5
3
f
x 10^-4
LR
Lm
dx

amplitude of the displacements of potential temperature contours increase, so does the component of vertical velocity w.

The potential temperature and w fields for each f used in our numerical experiments are shown in Figs. 4.4 and 4.5 respectively.

We can see clearly defined vertically propagating gravity waves for each value of f (Fig. 4.4) and as f decreases the amplitude of the displacement of the isentropes appears to increase. The flow becomes more turbulent and is very turbulent for $f = f_0/4$ (Fig. 4.4(d)), however the flow for $f = 0$ (Fig. 4.4(e)) is not as turbulent as this. The w fields (Fig. 4.5) also clearly show the vertically propagating gravity waves and the maximum value of w appears to increase as f decreases. Therefore, we expect that as f decreases, the vertical kinetic energy increases.

A diagnostic calculation of the vertical kinetic energy is performed using (4.3). Above the mountain top the vertical KE of the balanced flow is negligible and so we use this as a measure of the gravity wave activity. Below the mountain top even the balanced flow implies large vertical KE. The region above the mountain over which we calculate the KE is the same size for each solution and is defined by

$$\begin{cases} 1 \times 10^6 m < x < 4 \times 10^6 m,\ 4000m < z < 10000m & f = 0, 2f_0, f_0, f_0/2 \\ 2 \times 10^6 m < x < 5 \times 10^6 m,\ 4000m < z < 10000m & f = f_0/4 \end{cases}$$

At each grid point in the region ρw^2 is evaluated and all values added together to calculate the total vertical KE. The variation of this energy with f is shown in Fig. 4.6.

As expected we see that the vertical KE increases as f decreases, however the value for $f = 0$ is less than that for $f_0/4$. This may be further evidence of the singularity of the limit $f \to 0$ (previously discussed in Section 4.1 in that the solution does not converge with decreasing f to the $f = 0$ state.

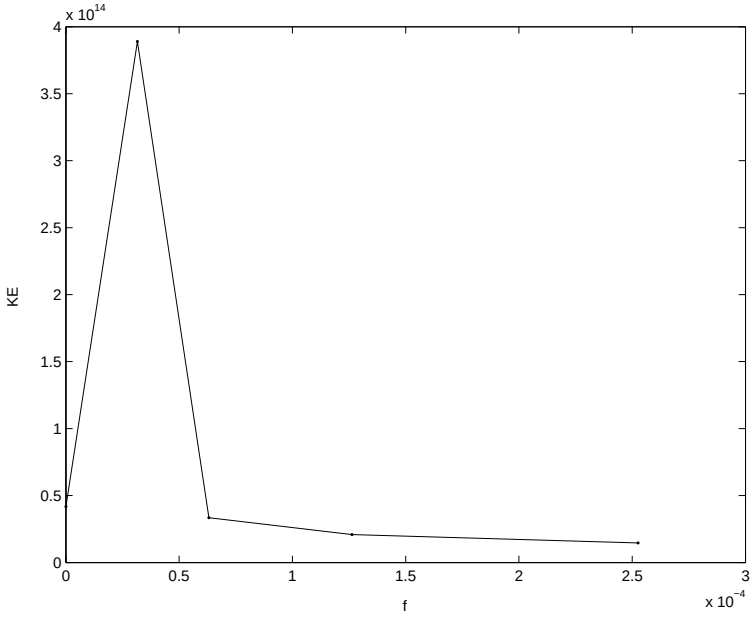

Figure 4.6: *Variation of vertical kinetic energy with Coriolis parameter f.*

4.4 Variation of pressure drag with f

Wind speed tends to be low on the windward slope of a mountain or ridge and faster on the leeward slope. From Bernoulli's equation, this requires a pressure difference across the mountain—high pressure upwind and lower pressure downwind (Smith 1979a) . The pressure difference results in a net drag on the mountain which can be computed as the horizontal pressure force on the mountain

$$D = \int_{-\infty}^{\infty} p(x, z = 0) \frac{dr}{dx} \, dx \tag{4.4}$$

where r is a height coordinate.

For the balanced solution there is drag due to upstream blocking (Shutts 1998), then for larger Ro there is additional wave drag.

The effect of rotation is to reduce the drag. As the parameter $Ro^{-1} = Lf/U$ increases, the flow gradually loses its wavelike character in the vertical plane (Smith 1979b). Ólafsson and Bougeault (1997) consider the fluid being decelerated as it approaches the mountain. The deceleration weakens the Coriolis force, and there is a net force acting to turn the flow

left. Kinetic energy is transferred from flow in the x direction to flow in the y direction. The movement along the x axis sources the kinetic energy that counteracts the buoyancy force and forms the mountain wave. Therefore one may expect less pronounced waves in the presence of rotation.

In our experiments the drag on the mountain is calculated on the bottom row of the domain using an approximation to (4.4), i.e.

$$D = \sum_{i=0}^{\frac{J}{2}} p_i \left(\frac{r_{i+1} + r_i}{2} - \frac{r_{i-1} + r_i}{2} \right) - \sum_{i=\frac{J}{2}}^{J} p_i \left(\frac{r_{i+1} + r_i}{2} - \frac{r_{i-1} + r_i}{2} \right) \tag{4.5}$$

where $i = 0$ is the left hand edge of the mountain base, $i = J$ is the right hand edge of the mountain base and $\frac{J}{2}$ is the centre point of the mountain.

Chapter 5

Sensitivity of Solution to upstream flow speed U

For the experiments in this chapter standard values of $f = f_0$ and $N = 0.01s^{-1}$ are used and U is varied according to the values given in Table 3.2. Thus as U decreases, Ro and Fr decrease at the same rate.

5.1 Variation of vertical kinetic energy with U

Smith (1979a) considers the limit of very slow wind speeds and strong stratification so that Fr is small. In this situation there will be little vertical motion and the fluid particles will deflect horizontally. He states that as Fr increases vertical deflections will occur. We could then argue that the vertical kinetic energy will also increase.

Sprenger and Schär (2001) conducted experiments in the rotating case where the upstream flow speed was varied from a standard value of $10ms^{-1}$ to values of $5ms^{-1}$ and $20ms^{-1}$. They noted that in general, a decrease of the upstream velocity inhibited wavelike features downstream. So we expect to find that as we decrease U, the amplitude of the displacement of the isentropes decreases. Thus the component of vertical velocity w should also decrease. In our experiments we again use (4.3) to calculate the vertical KE in a region above the mountain. We have said previously that this is a measure of gravity wave activity and so we should find that the vertical KE too decreases with decreasing

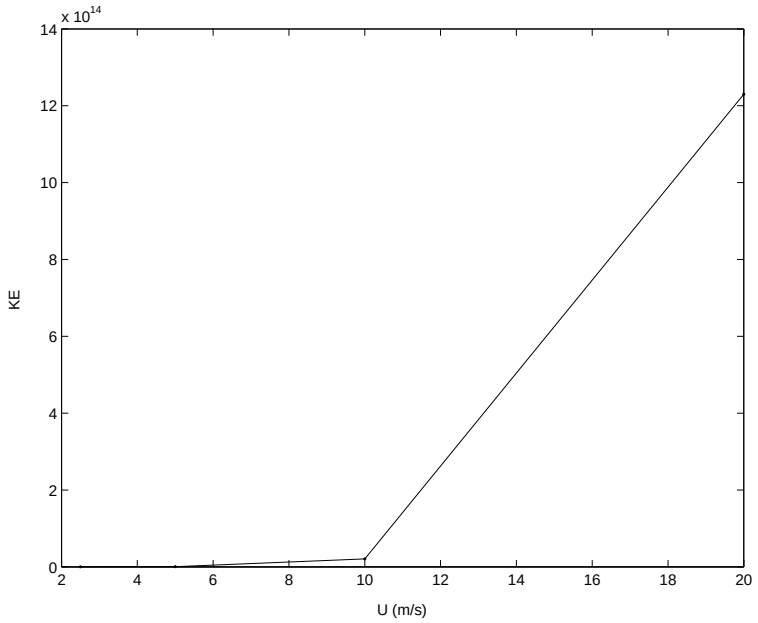

Figure 5.3: *Variation of vertical kinetic energy with upstream flow speed U.*

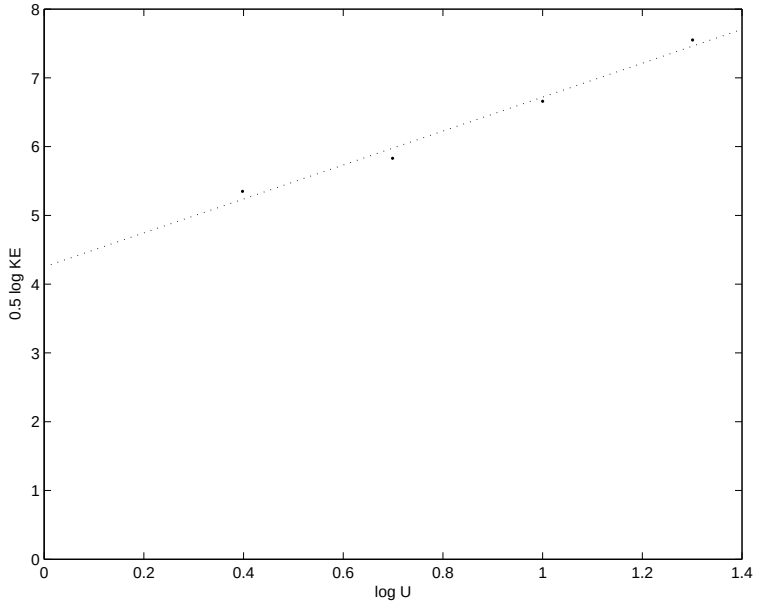

Figure 5.4: *Variation of $\frac{1}{2} \log KE$ with $\log U$. The equation of the line of best fit is $\frac{1}{2} \log KE = 2.468 \log U + 4.250$.*

5.2 Variation of pressure drag with U

In Section 4.4 we found that pressure drag increased as f decreased, i.e. as Ro increased. Since $Ro = U/fL$ and f remains constant in the experiments here, we could expect that as U increases, pressure drag also increases. Experiments conducted by Smith (1979b) showed that as the incident velocity decreased, so did the drag. This is indeed the case for our numerical experiments as shown in Fig. 5.5, yet it is only a weak dependence. Again Eq. (4.5) is used to compute the pressure force on the mountain. We see a reasonably linear relationship as U decreases from $20ms^{-1}$ to $5ms^{-1}$. However, the drag is slightly increased for $U = 2.5ms^{-1}$.

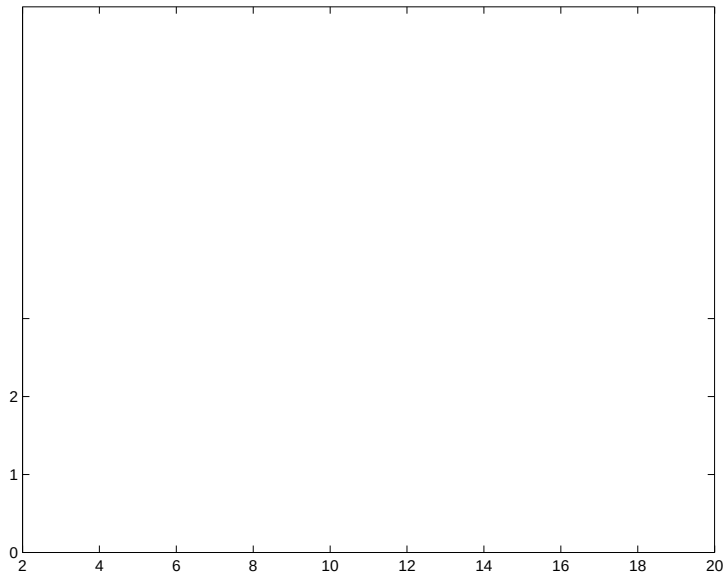

Chapter 6

Sensitivity of Solution to Rotation and Stratification

For the experiments in this chapter we vary the values of f and N but keep the value of the dimensionless parameter f/N constant. Using standard values of $f_0 = 1.263 \times 10^{-4} s^{-1}$ and $N_0 = 0.01 s^{-1}$ we get a value of $f/N = 0.01263$. Therefore, experiments are conducted using $2f_0$ and $2N_0$, f_0 and N_0, $f_0/2$ and $N_0/2$, and $f_0/4$ and $N_0/4$. Thus Ro and Fr increase at the same rate.

6.1 Effect on upstream influence distance and barrier jet

From the equation for the Rossby radius of deformation, L_R (4.1) we see that since we are keeping f/N constant, this theoretical value will remain at $190km$. In our experiments, the model distance of upstream influence, L_m, is calculated as described in Section 4.2 and the additional measure, δx (4.2) is also calculated. The variation of these are plotted against what we term the 'scaling factor' in Fig. 6.1 and the constant value of L_R is also shown for comparison. The scaling factor is just the factor of both f and N used in each experiment.

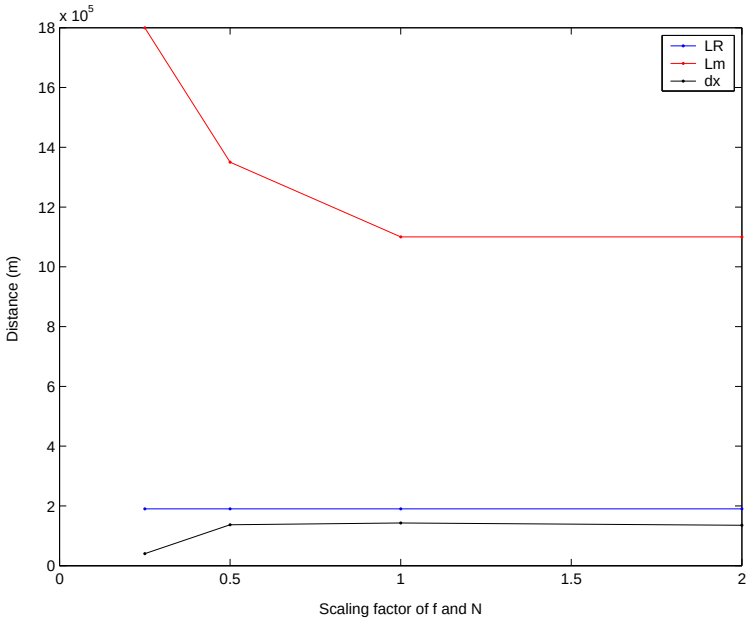

Figure 6.1: *Variation of distance of upstream* - . c :

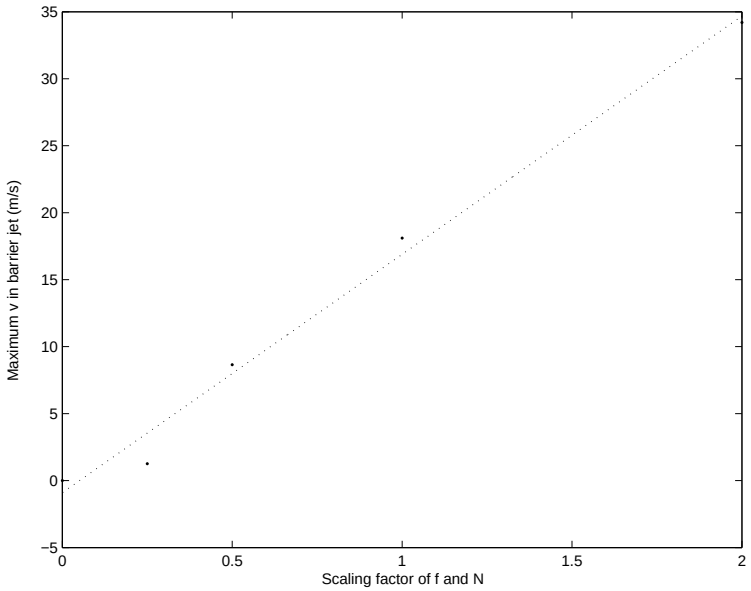

Figure 6.3: *Variation of v_{max} with scaling factor. The equation of the line of best fit is* $v_{max} = 17.8S_{f,N} - 0.903$.

Therefore, we could conclude that f/N is a useful parameter for determining the strength of the barrier jet.

6.2 Effect on vertical kinetic energy

As we have already seen from Section 4.3 that the effect of increasing Ro without any change in N is an increase in vertical kinetic energy. Here, we are also varying N and so Fr becomes an important parameter. We have already argued in Section 5.1 that with increasing Fr the vertical KE also increases. Therefore as we increase N we expect the vertical KE to decrease.

Figures 6.4 and 6.5 show the θ and w fields for the experiments in this chapter. Note that we have rearranged the panels so that Fig. 6.4(a)-(c) can easily be compared to Fig. 5.1(a)-(c) respectively. The solution in Fig. 6.4(d) does not reproduce the same Ro and

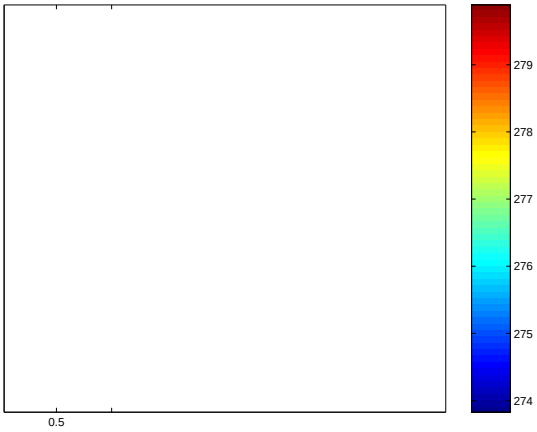
279
278
277
276
275
274
0.5

KE is still substantial but less than for the $S_{f,N} = 1/2$ case. This could again be due to the apparent reduction in gravity wave activity as discussed above.

The scaling factors 2, 1 and 0.5 correspond to $Ro = 0.13$, 0.26 and 0.53 respectively. The trend of the vertical kinetic energy between these points compare swell to the points corresponding to $U = 5$, 10 and 20 in Fig. 5.3. We expect this to be the case.

We could conclude that f/N is a useful parameter for investigating gravity wave activity.

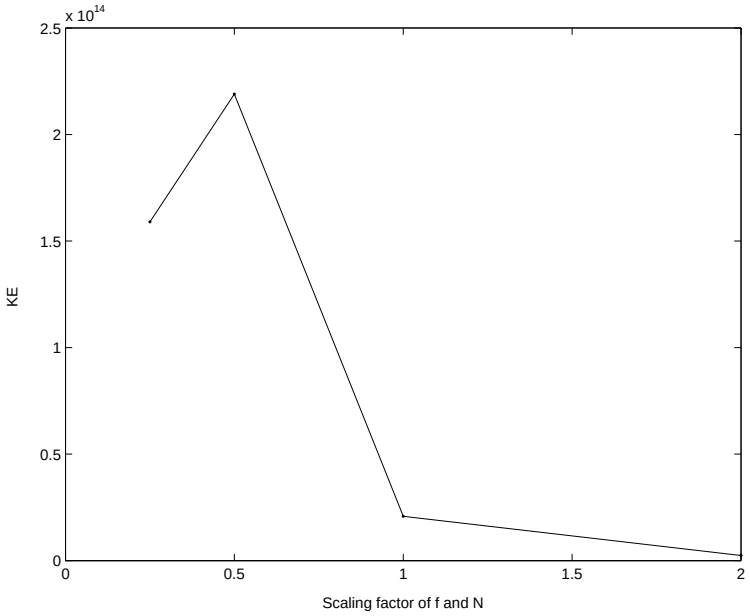

Figure 6.6: *Variation of vertical kinetic energy with scaling factor.*

6.3 Effect on pressure drag across the mountain

Figure 6.7

The points corresponding to $S_{f,N} = 1$ and 0.5 agree extremely well with the points corresponding to $U = 10$ and 20 in Fig. 5.5. The point for $S_{f,N} = 2$ does not compare so well with $U = 5$.

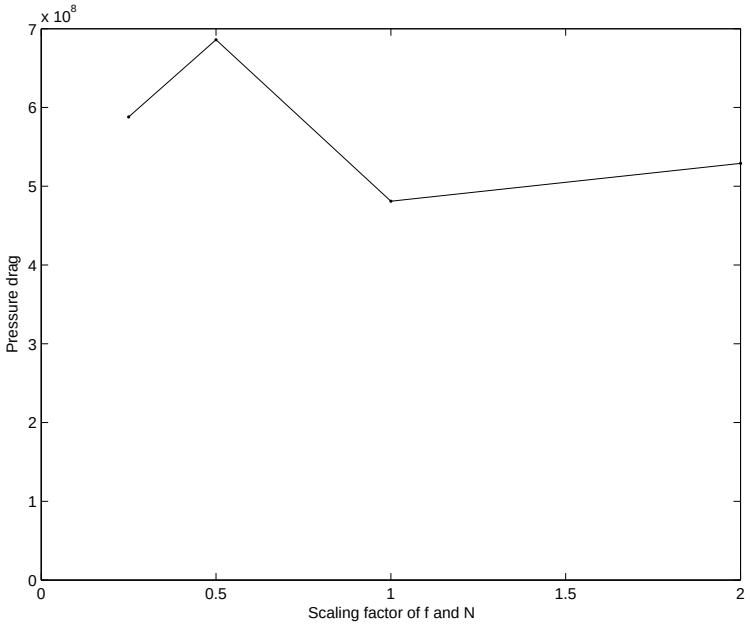

Figure 6.7:

Chapter 7

Discussion

A vertical slice version of the Met Office Unified model has been used to investigate the flow over an isolated cosine mountain. The stratification, N, and upstream flow speed, U, are both constant with height. The project aimed to simulate some of the features of flows over orography by varying just three dimensionless parameters. These were the Froude number ($Fr = U/NH$), Rossby number ($Ro = U/fL$) and ratio (f/N).

One of the main results of the project is that the limit $f \to 0$ is singular, i.e. the v fields of the flow solution did not converge towards the $f = 0$ solution. It also has multiple solutions; one for $f = 0$ and two obtained in the limits $f \to 0^+$ and $f \to 0^-$.

A well defined barrier jet exists even for small value of f because, from the horizontal momentum equation, a weak pressure gradient will still exist. As both f and N are scaled up the strength of the barrier jet increases linearly with the scaling factor. This suggests that the dimensionless parameter f/N is useful for determining the strength of the barrier jet. The barrier jet exists within the distance of upstream influence. The distance $\delta x = v_{max}/f$ agrees well with the theoretical Rossby radius of deformation, L_R, as f varies but the model upstream distance, L_m, differs substantially from both of these.

Vertical kinetic energy is used as a measure of gravity wave activity above the mountain. The amplitude of these waves increases as f decreases, however, for the $f = 0$ case the wave activity is less than for the $f = f_0/4$ case. Thus, we see that the vertical kinetic energy increases as f decreases apart from when $f = 0$ when it is much less than when

$f = f_0/4$. As f and N are both scaled down the gravity wave activity increases. In the case of decreased N, vertical displacements with increased amplitude become more possible. When $f = f_0/4$ and $N = N_0/4$, Ro and Fr exceed 1 and gravity wave activity appears to lessen. Therefore, vertical kinetic energy increases as the scaling factor decreases, apart from when the factor becomes less than 1/2 when the energy begins to decrease.

By decreasing U with all other parameters held constant, Ro and Fr are decreased at the same rate. As Ro decreases wave activity decreases and the solution gets closer to

References

Baines, P. G. 1987 Upstream blocking and airflow over mountains. *Ann. Rev. Fluid Mech.*, **19**, 75-97

C

Pierrehumbert, R. T. and Wyman, B.	1985	Upstream effects of mesoscale mountains. *J. Atmos. Sci.*, **42**, 977-1003
Quaile, E. L.	2001	Föhn and chinook winds. *Weather*, **56**, 141-145
Shutts, G.	1998	Idealised models of the pressure force on mesoscale mountain ridges. *Contrib. Atmos. Phys.*, **71**, 303-313
Smith, R. B.	1979a	The influence of mountains on the atmosphere. *Adv. Geophys.*, **21**, 87-230
Smith, R. B.	1979b	The influence of the earth's rotation on mountain wave drag. *J. Atmos. Sci.*, **36**, 177-180
Smith, R. B.	1989	Hydrostatic airflow over mountains. *Adv. Geophys.*, **31**, 1-41
Sprenger, M. and Schär, C.	2001	Rotational aspects of stratified gap flows and shallow föhn. *Q. J. R. Meteorol. Soc.*, **127**, 161-187

Acknowledgements

I would like to thank Professor Mike Cullen for his advice and guidance throughout the duration of this project and also thanks to Dr Pete Sweby and Sue Davis for all their assistance over the past year. Thanks are also due to my family who encouraged me that it was the right thing to do the course.

Thanks to Andy for helping me get rid of stress during many juggling sessions. Huge thanks go to Sal, for all her support and encouragement.

I also thank NERC for their financial support.

Declaration

'I confirm that this is my own work and the use of all material from other sources has been properly and fully acknowledged.'